Simulation and Analysis of Flow Through Micro Channel

[1]Madhusree Kundu,[*] [2]Krishna Vamsee, [3]Dilip Maiti

[1] Department of Chemical Engineering, NIT Rourkela, Orissa-769008
[2]Chemical Engineering Group, BITS, Pilani, Rajasthan 333-031
[3] Mathematics Group, BITS, Pilani, Rajasthan 333-031

ABSTRACT

One-dimensional and two-dimensional models for microchannel flow with non-continuum (slip-flow) boundary conditions have been presented here. This study presents an efficient numerical procedure using *pressure-correction-based* iterative SIMPLE algorithm *with QUICK scheme in convective terms* to simulate a steady incompressible two-dimensional flow through a microchannel. In the present work, the slip *flow* of liquid through a microchannel has been modeled using a slip length assumption instead of using conventional Maxwell's slip flow model, which essentially utilizes the molecular mean free path concept. The models developed; following this approach lend an insight into the physics of liquid flow through microchannels.

Keywords: microchannel, slip-length, Hagen-Poiseuille, Monge's method, SIMPLE, *QUICK,* friction factor.

[*] Corresponding author, E-mail:mkundu@nitrkl.ac.in, madhushreek@yahoo.com
Fax: 0661-2462999

1. INTRODUCTION

Micro fluidics is an area of science and engineering in which fluid behaviour differs from conventional flow theory primarily due to non-continuum effects, surface dominated effects, and low Reynolds number effects induced by the small length scale of the micro flow systems. With the recent achievements in the field of nanotechnology, microprocessor chip cooling, patterned drug delivery and biotechnology, the microfluidic devices are becoming more prevalent both in commercial application and in scientific inquiry. The classification proposed by Mehendale *et al*.[1] and Kandlikar and Grande [2] categorized the range from 1 to 100μm as microchannels. In microfluidics, theoretical knowledge for gas flows is currently more advanced than that for liquid flows [3]. Concerning the gas flow through microchannels, the issues are actually more clearly identified; the main micro-effect that results from shrinking down of device size is 'rarefaction'. In the continuum fluid transport theory, governed by the Navier-Stokes equations, it is assumed that the state variables do not vary appreciably over the length and time scales compared to the molecular mean free path and molecular relaxation time. The local density oscillation near the solid-liquid interface of the microchnnels, significant deviation of liquid viscosity compared to the bulk value may not necessarily mean the breakdown of continuum theory; at the same time it is important to understand how the continuum theory works in a micro flow. There were no evidences that continuum assumptions were violated for the microchannels tested, most of which had hydraulic diameters of 50 μm or more. There is a clear need for additional systematic studies which carefully consider each parameter influencing transport in microchannels [4]. In general, there seems to be a paradigm shift in the focus of published articles from

descriptions of the manufacturing technology to the discussions of the physical mechanisms of flow and heat transfer through microchannels[5, 6]. Sobhan and Garimella [4] have made a comprehensive review on investigations regarding the flow and heat transfer characteristics for microchannel flow.

Apart from wetting, adsorption and electrokinetic effects, the slip phenomena play an important role in modeling liquid flow through microchannel [7]. Helmloltz and Von Piotrowski found evidence of slip between a solid surface and liquid and later Brodman [8] verified their results [7]. Navier[9] was the first to model partial slip at the wall for liquids well before Maxwell's slip model for gases [7]. Slip length is the distance behind the solid-liquid interface at which the velocity extrapolates to zero. An interpretation of the slip length (L_S) is shown in Fig.1. The validation of slip boundary conditions continued in the beginning of the twentieth century, with a focus mostly on flow through capillaries. Traube and Whang [10] reported 4-5 fold increase in flow rate of water in a capillary treated with oleic acid. This increment could be attributed either to boundary slip or simply as surface tension induced capillary rise. The systematic study undertaken by Schnell [11], who used water in glass capillaries (240-800 μm) treated with silicone to make them hydrophobic found that for a small pressure drop in the capillary; the flow rate was lower in the treated cases compared to the untreated ones, but at the higher pressure drop the experience was opposite. Moreover, with the onset of turbulence there was no discernible difference in flow rates. Schnell's experiments stood the test of time and are considered as the first convincing proof of boundary slip occurring for water flow on hydrophobic surfaces. At about the same time, Debye and Cleland [12] established that the boundary slip can also occur in liquid hydrocarbon flow through porous vycor glass.

In the last few decades there has been a renewed interest in determining the validity of the no-slip boundary condition for liquids due to the interest in polymers and other complex fluids but primarily due to microfluidic applications. The effective use of the surface force apparatus (SFA) in the 1990's has led to many interesting experimental results and detailed studies of boundary slip with water and other substances [7]. Liquid flow in a microchannel becomes fully developed after a short entrance length, so that it can be modeled as a two-dimensional flow [13]. In view of this, present study aims for one-dimensional and two-dimensional microchannel flow simulation with non-continuum (slip-velocity) boundary conditions, in general. The present paper is focused on analyzing the effect of two-dimensional dependency of velocity, compressibility of liquid flow through a microchannel on a simple analytical and computational fluid dynamics perspective.

Majority of the experimental works indicate a strong dependence of the slip length on the approach rate (and thus shear rate) and wall roughness of the microchannels. Very large values of slip length, of the order of hundreds of nanometers were reported in the open literature [7]. Tretheway and Meinhart [14] used micro particle image velocimetry (PIV) to measure the velocity profiles of water in 30 x 300 µm channel. The channel surfaces were treated with a 2.3 nm OTS (octedecyltrichlorosilane) layer. The velocity profiles were measured in a 25 x 100 µm plane to within 450 nm of the channel wall. A slip velocity of about 10 % of the maximum velocity was measured, which corresponds to slip length of about 1µm. This large value of slip length is typically encountered in polymer flows [7]. Choi *et al.* [15] reported slip length of 30 nm at the shear rate of 10^5 s^{-1} in OTS coated 500 µm wide x 9 mm long microchannels of heights 0.5

μm and 1.0 μm. In case of hydrophilic surfaces of the same channels and for the same shear rate they reported a slip length of 5 nm. Molecular dynamic (MD) simulation predicts the slip length to be roughly 1/10 th of the experimental results. These large discrepancies have been addressed with the help of a few conceptual slip models like 'Molecular slippage' model considered by Blake [16]; 'Gaseous film' model proposed by Ruckenstein and Rajora [17]; 'Viscosity model' proposed by Vinogradova [18]; ' No-shear/No-slip patterning' presented by Phillip [19]. In the gaseous film model, it was assumed that there may be a film of gas at the interface between solid surface and liquid. The origin of this film may be the externally dissolved gases up to metastable concentrations. According to deGennes [20] this gas film nucleates bubbles preferentially near the wall at contact angles greater than 90^0, i.e., on hydrophobic surfaces. Evidences of nano bubbles on a hydrophobic glass surface in water using atomic force microscope were reported by Tyrrell and Attard [21]. Thickness of the gaseous film was assumed to be less than 0.5 nm. deGennes [20] proposed a simple mathematical model for calculating slip length involving gaseous film thickness and physical properties of the fluid concerned and postulated a slip length of few microns for liquid flow through microchannel. The 'Viscosity model' proposed by Vinogradova was inspired by the slip mechanism in polymer melts. It provides a relation between the slip length and a decrease in viscosity within a very thin boundary layer δ close to a hydrophobic surface. He proposed a model for slip length ($slip\ length, b = \delta\left(\frac{\mu_b}{\mu_s} - 1\right)$, where μ_b is bulk viscosity and μ_s is a near wall viscosity). According to him there may be two mechanisms; instrumental for a large slip length, either large increment of δ or very high viscosity ratio. On the basis of the discussion so far about 'slip length', the authors think that in the present problem

choosing a value of slip length as clearance length (b)/100 for micro flow simulation will not contradict any physical institution.

Modeling the micro flows, specially for the gases require the mean molecular diameter *d*, the mean molecular spacing δ and the mean free path λ. For dilute gases $\frac{d}{\lambda}$ is less than 1 and different collision models based on this assumption determines the value of λ, which when divided by the channel characteristic length gives rise to a very important parameter Knudsen number for flows in microchannels. In the present work the conventional Maxwell's slip flow model was not used, which essentially utilizes the mean free path, and does not require a slip length assumption. An analogue to molecular mean free path the 'molecular diffusive path' has been proposed here using a slip length assumption to define a modified Knudsen number for liquid flow through micro channel.

2. A MOTIVATING EXERCISE

2.1 *One-Dimensional Flow Through Microchannel*

In this problem, as envisaged in Fig.2, the microchannel is viewed as two parallel plates placed one over the other extending into the z-direction and the flow is in the x-direction. It has been assumed that the z-directional dimension is equal to unity. The channel clearance length (b) is 0.1 mm or 100 μm. So far as the bulk properties of the fluids are concerned, 100 μm is still a scale governed by the classical laws of simple liquids and ideal gases under normal pressure. Therefore for ordinary liquids (fluids), the current micro fluidic device is subjected to the rules of classical fluid mechanics [22, 23].

Assumptions in the analysis

1. All the liquid properties viz., density, viscosity etc., are constant.
2. The fluid is newtonian in nature.
3. The flow is laminar and the shear rates involved are small.
4. The pressure gradients in all the directions, except in x direction are zero.
5. To simplify the problem, we consider the flow only in the x-direction and all the other directional velocities to be zero.

$$V_x = V_x(y), \qquad V_y = V_z = 0 \;, \quad p = p(x) \tag{1}$$

Classical fluid mechanics for macrochannels is based on n*o-slip* boundary condition. At the walls of the microchannel, the velocity of the fluid is given by

$$V_x\big|_{wall} = L_S\left(\frac{\partial V_x}{\partial n}\right)_{wall} \tag{2}$$

where, L_s is slip length and **n** is the normal coordinate pointing *inward* from the channel wall. Slip-length can be referred to as extrapolation length; it is the distance from the wall at which the fluid is assumed to attain the normal parabolic velocity profile. The equations to be used to get the velocity profile are continuity and Navier-Stoke's equations along with the boundary condition (Eqn (2)) to get the velocity profile as follows,

$$V_x = \frac{1}{2\,\mu}\frac{dp}{dx}\left[y^2 + (-b)(y + L_S)\right] \tag{3}$$

Equation (3) is the starting equation for the analysis of one-dimensional velocity problem considered here, characterized by low-shear rates and negligible pressure gradients in directions other than the flow direction.

Experiments conducted by Choi et. al. [24] on hydrophobic surfaces, where the shear rates involved are high, has indicated that L_S depends upon velocity gradient, which in turn depends upon the flow-rate through the channel.

$$L_S = 0.192\left(\frac{dV_x}{dy}\right)_{wall}^{0.46} \tag{4}$$

By equating Eqn (3) to zero and solving the resulting quadratic equation, the value of 'y' can be determined. The channel clearance, b has already been taken as a constant, not varying either with the flow-rate or the working fluid. The slip-length can be assumed to be constant at any arbitrary point on the walls of the channel owing to its dependence on velocity gradient as given by the Eqn (4) and the velocity gradient is essentially constant at any arbitrary point on the x-axis or on the walls.

Average velocity is defined here as the ratio of flow-rate along the x-axis direction of the channel to the cross-sectional area normal to the direction of flow i.e., the y-z plane. Mathematically, it can be expressed as

$$\langle u \rangle = \frac{-b}{2\,\mu}\frac{dp}{dx}\left[L_s + \frac{b}{6}\right] = Q/A = Q/b \tag{5}$$

Where Q is the volumetric flow rate through the channel. This average velocity $\langle u \rangle$ is used to obtain the pressure distribution along the x-direction, also referred to as Hagen-Poiseuille's equation (Eqn (5)),

$$p_i - p_f = \frac{2\mu LQ}{b^2\left(\frac{b}{6} + L_s\right)} \tag{6}$$

It can be rearranged in the following form,

$$\Delta p = \frac{4\left(\frac{\mu}{G}\right)}{\left(L_s + \frac{b}{6}\right)}\left(\frac{G\langle u\rangle}{2}\right)\left(\frac{L}{b}\right) \tag{7}$$

Where, G and $\langle u\rangle$ are the mass and average velocities, respectively, through the channel. The RHS of Eqn (7) has been expressed as a function of '$\left(\frac{L}{b}\right)$' and the kinetic head and it can be conveniently expressed as

$$\Delta p = f_m \frac{\rho\langle u\rangle^2}{2}\left(\frac{L}{b}\right) \tag{8}$$

where, f_m can be thought of as the friction factor on the basis of average velocity of the channel. Kinetic theory predicts that mass and momentum diffusivity is given by the same expression at very low mass concentration of molecular flow,

$$\begin{aligned} \nu &= {\langle u\rangle \lambda}/{3} = D \\ \Rightarrow \lambda &= \frac{3\nu}{\langle u\rangle} = \frac{3}{{\langle u\rangle}/{\nu}} = \frac{3\mu}{G} \end{aligned} \tag{9}$$

where, λ is the mean free path of the fluid molecules inside the channel. ν and D are the momentum and mass diffusivity, respectively. f_m, the friction factor can be expressed as

$$f_m = \frac{\left(4{\mu}/{G}\right)}{\left(L_s + \frac{b}{6}\right)} = \frac{\left(4{\lambda}/{3}\right)}{\left(L_s + \frac{b}{6}\right)} \tag{10}$$

It is also evident from Eqns (7) and (10) that the pressure required to drive the fluid is lesser in microchannel than in comparison to macrochannel.

2.2 One-Dimensional Flow Through Microchannel With A Two-Dimensional Velocity Field

In this problem, the emphasis will be on a velocity, which is dependent upon both the radial as well as the axial dimensions of the same microchannel as considered in Fig. 2.

Assumptions

1. The fluid is Newtonian in nature with constant viscosity.
2. The flow is laminar and the shear rates involved are small.
3. For small flow rates, we have

$$u = u(x, y) \; and \; v = w = 0 \tag{11}$$

On substitution of the boundary conditions, the pressure distribution becomes

$$p = p(x) = \lambda_0 \frac{x^2}{2} + a_1 x + a_2 \tag{12}$$

The pressure gradient in the radial direction is neglected because of the small radial dimension.

2.2.1 Equations to be used

The equation of continuity becomes (adhering to the postulates taken)

$$\frac{\partial(\rho u)}{\partial x} = 0 = \frac{\partial(G)}{\partial x} \tag{13}$$

where, G is the mass velocity and constant along the axial direction. The axial directional momentum equation is rearranged in such a way that it gets into the 'normal form' of a partial differential equation which is given below

$$\frac{4}{3}\mu \frac{\partial^2 u}{\partial x^2} + (-\mu)\frac{\partial^2 u}{\partial y^2} = \left(-\frac{\partial p}{\partial x} - G\frac{\partial u}{\partial x}\right) \tag{14}$$

The radial directional momentum equation gives,

$$\frac{\partial^2 u}{\partial y \partial x} = 0 \tag{15}$$

There are numerous analytical methods for solving a partial differential equation out of which Monge's method is a veteran one [25]. This method essentially involves disintegration of the given partial differential equation into a set of three equations called as the Monge's equations which when solved give the first integral(s) of the equation. These first integrals are then used to calculate the variable in question. The partial differential equation (Eqn (14)), spitted into the set of Monge's equations is as follows,

$$\frac{4}{3}\mu\, dmdy - \mu dndx + \left(\frac{dp}{dx} + Gm\right)dxdy = 0 \tag{16}$$

$$\frac{4}{3}\mu\, dy^2 - \mu dx^2 = 0 \tag{17}$$

$$du = mdx + ndy \tag{18}$$

Where, $m = \frac{\partial u}{\partial x}, n = \frac{\partial u}{\partial y}$. Equation (16) can be rearranged in terms of first order partial differential equations in 'm' and 'n' and can be easily integrated. Once the integral equations are obtained for 'm' and 'n', they can be substituted into the Eqn (18) and solved for the velocity, which is as follows,

$$u = -\frac{\Delta p}{G} + \frac{\lambda_1}{K^2}e^{-kx} + \lambda_2 x + \left(\frac{dp}{dx} + Gm\right)\frac{y^2}{2\mu} + \lambda_3 y + \lambda_4 \tag{19}$$

where, $K = \frac{3G}{4\mu}$. The four constants can be solved with the following boundary conditions.

- **Axial :-**

$$u(0, y_0) = \langle u \rangle$$
$$\left(\frac{\partial u}{\partial x}\right)_{x_0 = 0} = 0 \tag{20}$$

- **Radial :-**

$$u(x_0,0) = L_S\left(\frac{\partial u}{\partial y}\right)_{y=0} \tag{21}$$

$$u(x_0,b) = -L_S\left(\frac{\partial u}{\partial y}\right)_{y=b} \tag{22}$$

The above boundary conditions when applied on the Eqn (19) lead us to different equations linking the four constants involved in the expression. These four constants when duly substituted in Eqn (15) yield the equation for the velocity through a micro - channel with two-dimensional dependency (Eqn (23)).

$$u = \left[\frac{\left(\frac{GK}{2\mu}\right)\left(\Delta p/G - \langle u\rangle\right)\left(1-e^{-Kx_0}\right)}{Kx + \left[\frac{GKb}{2\mu}\left(y+L_S\right)-1\right]\left(1-e^{-Kx_0}\right)}\right]\left[y^2 - b\left(y+L_S\right)\right] \tag{23}$$

2.2.2 Analysis

It has been observed that in a microchannel, with the velocity depending on both the dimensions, it doesn't lose its parabolic radial dependency. One of the important aspects of the microchannel flow is the decrease in the axial dimension dependent velocity along the axial direction, which eventually ensures the maintenance of laminar flow in the channel. There is also a flattening of parabolic velocity profile along the channel length. 'K' is defined as (ignoring the constant), the ratio of average velocity to momentum diffusivity (the ratio of force due to acceleration to the kinetic energy accumulated during diffusion). The molecular mean free path λ can be related to K as $\lambda = \frac{9}{4K}$. A dimension-less number can now be thought of as the ratio of inverse of 'K' to the characteristic dimension of the channel, say 'b'.

$$Kn_{\mathrm{mod}ified} = \frac{1/K}{b} \tag{24}$$

This '$Kn_{\mathrm{mod}ified}$' has similarities with Knudsen number (Kn) for gas flow in micro channels, which is the ratio of mean-free path of the molecules to the characteristic dimension of the channel. '$1/K$' can be viewed as "mean diffusive path" of the fluid (liquid) particles in the microchannel. '$Kn_{\mathrm{mod}ified}$' may also be viewed as the ratio of viscous force to inertial force i.e. inverse of Reynolds number. For small value of $Kn_{\mathrm{mod}ified}$, the classical flow regime is ensured. For large values of $Kn_{\mathrm{mod}ified}$ or small values of 'K' the flow is shifting towards the microfluidics regime, hence, the axial dimensional dependency ('$K*x$') is equally important as its radial dimensional dependency. From equations (9), (10), (24), the relation between 'K' and λ and the definition of 'K', the friction factor f_m in the microchannel can be viewed as

$$f_m = \frac{\left(4\mu/G\right)}{\left(L_s + \frac{b}{6}\right)} = \frac{\left(4\lambda/3\right)}{\left(L_s + \frac{b}{6}\right)} = 3\,Kn_{\mathrm{mod}ified} = \frac{3}{K\left(L_S + b/6\right)} \tag{25}$$

Due to the existence of slip length, there is a smoothening of flow in microchannels as is evidenced by the reduced value of friction factor in comparison to the value of friction factor in macrochannel with no-slip$\left(f = \frac{64}{\mathrm{Re}}\right)$.

3. TWO-DIMENSIONAL INCOMPRESSIBLE FLOW THROUGH MICROCHANNEL WITH A TWO-DIMENSIONAL VELOCITY FIELD

Assumptions

1. The fluid is newtonian in nature with constant viscosity and is 'incompressible'.
2. The flow is laminar and the shear rates involved are small.
3. Gravity effects are neglected.

4. We also assume that, $\bar{u} = \bar{u}(x, y), \bar{v} = \bar{v}(x, y), \bar{w} = 0$

We expect the radial direction flow to be purely pressure driven and so pressure gradients in both axial as well as radial directions exist.

3.1 Governing Equations:

Steady two-dimensional Navier-Stokes equations for a constant property fluid in non-dimensional conservative form are given by

$$\frac{\partial u}{\partial x} + \frac{\partial v}{\partial y} = 0 \tag{26}$$

$$\frac{\partial u^2}{\partial x} + \frac{\partial uv}{\partial y} = -\frac{\partial p}{\partial x} + \frac{1}{\mathrm{Re}}\left(\frac{\partial^2 u}{\partial x^2} + \frac{\partial^2 u}{\partial y^2}\right) \tag{27}$$

$$\frac{\partial uv}{\partial x} + \frac{\partial v^2}{\partial y} = -\frac{\partial p}{\partial y} + \frac{1}{\mathrm{Re}}\left(\frac{\partial^2 v}{\partial x^2} + \frac{\partial^2 v}{\partial y^2}\right) \tag{28}$$

Where the non-dimensional variables are defined as

$$x = \frac{\bar{x}}{b}, y = \frac{\bar{y}}{b}, u = \frac{\bar{u}}{U_\infty}, v = \frac{\bar{v}}{U_\infty}, t = \frac{\bar{t}\,U_\infty}{b}, p = \frac{\bar{p}}{\rho U_\infty^{\,2}} \tag{29}$$

The variables with bar denotes a dimensional variable. b is the channel clearence, U_∞ is the free-stream velocity, ν is the kinematic viscosity, ρ is the fluid density**,** and Re is

$$\mathrm{Re} = \frac{U_\infty b}{\nu} \tag{30}$$

3.2 Friction factor

The local friction factor f_{local} and average friction factor $\bar{f}$ are defined as

$$f_{local} = \frac{\tau_w}{\rho U_\infty^2 / 2} = \frac{2}{\mathrm{Re}}\left(\frac{\partial u}{\partial y}\right)_{wall} \text{ and } \bar{f} = \frac{1}{L}\int_0^L f_{local}\,dx \tag{31}$$

Where τ_w is the shear stress acting on the walls of the channel and L is the channel length.

3.3 Boundary Conditions

The boundary conditions (Eqns (33), (36), and (37)) are described in the following way. The slip velocity, u_w defined by Eqn (33), on the channel walls is based on the following assumptions,

a) At a distance of '$\overline{L_s}$' from the present channel wall, on both the sides, there exists an imaginary boundary wall' (IBW) – rigid and solid.

b) At the position where presently there exists a wall, it is assumed that no solid wall is present and there exists a velocity for the fluid moving over the 'imaginary boundary wall' (IBW). The velocity is equal to the slip-velocity in the present case.

Considering the above steps, it becomes clear that the flow over the 'imaginary boundary wall' (IBW) is shear flow. Extending this 'imaginary' case to a boundary layer problem 'completely' i.e., the case in which we intend to find the velocity profile of the moving fluid over the 'IBW'. The boundary layer theory of the classical mechanics can be safely used since the imaginary boundary, which is being considered here does not have any 'slip'.

Thus we obtain an expression for the velocity of the moving fluid over the 'IBW' as:

$$\overline{U} = U_\infty \left[\frac{3}{2}\left(\frac{\bar{y}}{\bar{\delta}}\right) - \frac{1}{2}\left(\frac{\bar{y}}{\bar{\delta}}\right)^3 \right] \tag{32}$$

We understand that the velocity at a distance of '$\bar{L}_s$' from the IBW should be the slip velocity (Fig. 1). So replacing '$\bar{y}$' with '$\bar{L}_s$' ($\bar{L}_s = \frac{b}{100}$) would yield us the slip-velocity as:

$$u_w = \frac{\overline{u_w}}{U_\infty} = U_\infty \left[\frac{3}{2}\left(\frac{\bar{L}_s}{\bar{\delta}} \right) - \frac{1}{2}\left(\frac{\bar{L}_s}{\bar{\delta}} \right)^3 \right] \tag{33}$$

The problem now is to find the 'free-stream velocity, U_∞' and the 'boundary layer thickness, $\bar{\delta}$. As we are dealing with microchannels it can be expected that the velocity of the fluid on the 'IBW' shall be small enough to consider the flow as 'laminar'. This consideration will yield the expression for the boundary layer thickness, $\bar{\delta}$ as:

$$\frac{\bar{\delta}}{\bar{x}} = \frac{5.0}{\sqrt{\mathrm{Re}_{\bar{x}}}} \tag{34}$$

Where,

$$\mathrm{Re}_{\bar{x}} = \frac{G\bar{x}}{\mu} = \frac{Gb}{\mu}\frac{\bar{x}}{b} = \mathrm{Re}_x\, x \tag{35}$$

The free-stream velocity (U_∞) is nothing but the incident velocity. Thus combining the above expressions, we get an expression for the slip-velocity as a function of $\bar{\delta}$ i.e., a function of '$\bar{x}$'. Mathematically it can be derived that the slip-velocity is actually an inverse function of axial dimension. The radial velocity component is assumed to zero on the channel walls.

At the entrance of the channel, the radial velocity component is set to zero, and a uniform velocity U_∞ for the axial velocity component is assumed.

$$\mathrm{u} \to 1, \mathrm{v} \to 0 \quad \text{at the entrance.} \tag{36}$$

Because of the elliptic nature of the flow fields investigated, the outlet boundary condition will have some influence on the development of the upstream flow. The normal gradient of all dependent variables at the outlet are constants. This is equivalent to the requirement of the second derivative of any dependent variable becoming zero (Eqn (37)). Using this condition the numerical procedure is stable and convergent for those flows, which eventually reaches a steady-state condition at the outlet [26].

$$\frac{\partial^2 u}{\partial x^2} = \frac{\partial^2 v}{\partial x^2} = 0 \tag{37}$$

3.4 Numerical Method

In this problem, a fictitious time derivative is introduced in the momentum equations. The pressure correction based iterative SIMPLE algorithm [27] has been used for solving the governing equations with the boundary conditions specified previously. The computational domain is divided into Cartesian cells. Staggered grid arrangements (Fig.3(a)) are used, in which velocity components are stored at the midpoints of the cell sides to which they are normal. The pressure is stored at the center of the cell. A first order implicit scheme is used for time derivative discretization. The u-momentum equation after integration over the u-control volume (Fig.3(b)) becomes

$$F_e\phi_e - F_w\phi_w + F_n\phi_n - F_s\phi_s = b \tag{38}$$

Where $\varphi = \mathrm{u}$ or v and F_e is the non-linear coefficient of ϕ_e. b contains the source terms, diffusive terms and time-derivative terms. The convective terms at any interface is estimated by a linear extrapolation of the ϕ_e values at two upwind neighbors, thus

$$F_e\phi_e = \left(\frac{3}{2}\phi_p - \frac{1}{2}\phi_w\right)\left[\left|F_e, 0\right|\right] - \left(\frac{3}{2}\phi_E - \frac{1}{2}\phi_{EE}\right)\left[\left|-F_e, 0\right|\right] \tag{39}$$

Where, the symbol $\left[\left|a, b\right|\right]$ represents the maximum of the two operands a and b. The diffusive terms at any interface is estimated by a linear interpolation between two grid point neighbors on either side of the interface. Thakur and Shy [28] discussed the 'upwind scheme' in detail. The pressure link between continuity and momentum is accomplished by transforming the continuity equation into a 'Poisson equation' for pressure. The Poisson equation implements a pressure correction for a divergent velocity field.

A single iteration consists of the following sequential steps:

1. An implicit calculation of the u, v momentum equations is performed through a block elimination method.
2. The Poisson equation for pressure correction is solved using a *Gauss-Seidel* iteration method with the *successive under relaxation* technique. In this case, the under-relaxation factor is chosen as 0.9.
3. The velocity field at each cell is updated using the pressure correction.
4. Convergence criteria is employed of the form

$$\left|\phi_{i,j}^{n+1} - \phi_{i,j}^{n}\right|_{\max} < \varepsilon \tag{40}$$

Here i and j denotes the cell index, n is the time level, ϕ is u or v. The value of ε is assumed to be 10^{-4}. Flow is assumed to start impulsively from rest. To facilitate the

convergence of the solution for a given higher Reynolds number (Re), the converged solution of a case with smaller Re is used as the initial guess.

3.5 *Grid consideration and algorithm testing*

A non-uniform grid distribution is incorporated in the computational domain. Fig. 4 shows the grid distribution inside the channel and at the entrance of the channel (up to $x = 10$). In order to resolve the gradients in a better way, the grid is finer near the channel walls and at the inlet. To check the grid sensitivity, we performed computations for four set of grids namely, 1500x150, 1000x150, 1500x100 and 1000x100; with the first and second number being the number of mesh points in the x-direction and in the y-direction, respectively. The maximum distance of the first grid point from each wall and from the entrance of the channel are $0.01b$ and $0.005b$, for the coarse and fine grids, respectively. The effect of grid size on the velocity profile at the centerline of the channel at various values of Reynolds number is presented in Fig. 7(b). We find that the change in solution for different grid size occurs on the third decimal place. We find that 1000x100 grids are optimum.

In order to assess the accuracy of our numerical method, we have computed 'Strouhal number' (St) for confined flow past a square cylinder in a channel for blockage ratio $\frac{B}{H} = 0.25$ where B is width of the square cylinder and H is width of the channel. In comparison to Mukhopadhyay *et al.* [29], the present study shows a maximum percentage deviation of 2.78 % in 'St'value at $\mathrm{Re} = 312$ (Fig. 5). Table 1 presents an excellent agreement among St and the time-average drag coefficient ($\overline{C_D}$) (experienced by the cylinder of height A and placed in a boundary layer of thickness δ at a gap height ratio

L from a wall) values calculated in the present work and those obtained by Hwang and Yao [30]. The boundary layer flow is generated from a uniform stream over a flat plate.

3.5 Flow simulation and discussion

Fig. 6 shows the radial velocity profile, along the radial direction at different x and $\mathrm{Re} = 10$. At the entrance of the channel, velocity in the radial direction is very small in comparison with that in the axial direction. It is evident from Fig.6 that after a certain value of x, at which flow has been fully developed, the change in radial velocity component is very negligible; it behaves as a one-dimensional flow.

Flattening in the velocity profile is a phenomenon has been found on the basis of one-dimensional flow problem as well as on the basis of numerical simulation of the two-dimensional flow considered here. Fig. 7(a) shows that along the length of a proper microchannel (b=1 mm, L=10 cm, with the slip boundary condition), at the centerline of it and for $\mathrm{Re} = 10$ the non-dimensional axial velocity develops to a value of 1.503 at x =1.21, the flattening in the velocity profile begins onwards. At about x=80 there is a constancy in u (longitudinal velocity) value (1.15) is reached. The effect of Reynolds number on flattening in longitudinal velocity profile is shown in Fig.7(b). From Fig. 7(a), it is evident that at a Reynolds number $(\mathrm{Re} = 1)$, the axial velocity is almost negligible at x=100, maintaining a slow rate of flattening with respect to space; hence, the compressibility can come into picture in order to satisfy continuity equation, though it is a liquid. A 'bottleneck' kind of effect may lead to a situation, where enormous amount of time will be required for the fluid to pass through the microchannel. At a Reynolds number $(\mathrm{Re} = 10)$, the flattening in axial velocity has been accelerated with respect to space and the axial velocity never ever reaches to such a negligible value. This flattening

in axial velocity is further accelerated for $(\mathrm{Re}=15)$ due to the high flow rate at the entrance, almost there is no flattening in u profile until x=100 for $\mathrm{Re}=15$. In order to avoid the 'bottleneck effect', which is also very much function of channel clearance, viscosity and elasticity of the fluid, an optimum value of Reynolds number has to be maintained for a microchannel flow.

The effect of Reynolds number on flattening of longitudinal velocity profile for a mini-channel (b=1 mm, L=10 cm, with no-slip boundary condition) and a proper macrochannel (b=10 cm, L=1 m, with no-slip boundary condition) has been compared in Fig.8. In a proper microchannel for $\mathrm{Re}=10$ the non-dimensional axial velocity develops to a value of 1.503 at x=1.21, then the flattening begins in the velocity profile. Whereas for mini channel, non-dimensional axial velocity develops to a value of 1.4935 at x =1.179 for $\mathrm{Re}=10$, then the flattening begins in the velocity profile. After the length of x=1.179, the mini-channel behaves like a proper microchannel. There is an earlier development of fully developed flow and a lower value of maximum longitudinal velocity component in mini-channel. Actually, it is the slip effect that delays the formation of fully developed velocity profile in proper microchannel with slip boundary condition. For the proper macrochannel the velocity profile could not be developed for same inflow rate within this channel span because $\mathrm{Re}_{macro}=\frac{b_{macro}}{b_{micro}}\mathrm{Re}_{micro}$ for the same inflow rate. It can be concluded that the flattening in the velocity profile in microchannel owes to the small scale of the dimensions of the channels involved.

The slip-velocity is independent of the radial component of the velocity. The slip velocity is a decreasing function of the axial dimension and has been found on simulation as shown in Fig.9. At x=10 and onwards the slip velocity is negligible, hence the channel

onwards behaving as a mini-channel, i.e., channel with micro dimension but with no-slip condition. This is also evident from Fig. 9 that the axial dimensional dependency of velocity (u), beside its radial dimensional dependency is to be considered within this short span of channel length for microchannels in practice.

The possibility of compression in liquid flowing through a microchannel is further strengthened from Fig. 10, which reveals that the non-linearity in pressure distribution with decreasing Reynolds number for a microchannel flow may cause compressibility effect. This non-linearity in pressure distribution, hence the corresponding compressibility effect, as discussed by Chen [13] in the numerical simulation for flow of gases through microchannels is much more pronounced than in comparison to the liquid micro flows. The curvature in pressure distribution curve for the slip flow is less than in no-slip flow because of reduced friction in case of slip flow.

Fig. 11 shows the simulated values of f. Re (f being the local friction factor & Re being the local Reynolds number) both for slip and no-slip conditions. The f. Re value for a slip value is much lower than a no-slip flow. This is due to the fact that slip effect reduces the wall friction significantly, hence, there is a reduction in driving pressure, again, which has been already predicted, based on the analytical solution of problems II and I.

4. CONCLUSIONS

Keeping in view of its immense significance, this paper is focused on the simulation and analysis of the microchannel flow. The narration of the microchannel flow behaviour should contribute to the theoretical understanding of such flows.

In microchannel, the velocity in the radial direction is small in comparison to that in the axial direction as is evident from the simulated results for a two-dimensional flow through it. After the flow has been fully developed, the change in radial velocity component is very negligible; it behaves as a one-dimensional flow. Flattening in the velocity profile is a phenomenon has been found on the basis of one-dimensional flow problem (II) as well as on the basis of numerical simulation of the two-dimensional flow considered here and it owes to the small scale of the dimensions of the microchannels involved.

At very low Reynolds number the axial velocity maintains a slow rate of flattening with respect to space; approaches to a negligible value; hence, the compressibility creeps in, to satisfy continuity equation, though it is a liquid. Slip velocity is a decreasing function of the axial dimension; hence, the channel after a certain length behaves as a mini-channel, i.e., channel with micro dimension but with no-slip condition. The axial dimensional dependency of velocity (u), beside its radial dimensional dependency is to be considered within this short span of channel length for microchnnels in practice.

The non-linearity in pressure distribution with decreasing Reynolds number for a microchannel flow may cause compressibility effect. The slip effect reduces the friction in microchannel flow hence fluid can be driven through it with a lesser power consumption than in comparison to the flow through macro or mini-channel.

ACKNOWLEDGEMENT

The authors are grateful to Prof. P. Tabeling & Prof. S. Garimella for some of their stimulating articles on microfluidics, which created the primary motivation behind the project undertaken. The authors are also indebted to Dr. B. Munshi, Department of

Chemical Engineering, NIT, Rourkela for his contribution in physical understanding of the problems undertaken.

REFERENCES

[1] S. S. Mehendale, A. M. Jacobi, and R. K. Shah, *Appl. Mech. Rev.*, **2003**, *53*, 175–193.

[2] S. G. Kandlikar, and W. J. Grande, *Heat Transfer Eng.*, **2003**, *24(1)*, 3–17.

[3] S. Colin, *Microfluidique*. Paris: Lavoisier – Hermès Science Publications, **2004**.

[4] C. B. Sobhan and S. V. Garimella, *Microscale Thermophys Eng.,* **2001**, *5*, 293-311.

[5] B. Palm, *Microscale Thermophys. Eng.,* **2001**, *5*, 155-175

[6] M. Gad-el-Hak, *J. Fluids Eng.,* **1999**, *12*, 5-33.

[7] G. Karniadakis, A. beskok, N. Aluru, *Microflows and Nanoflows Fundamentals and simulation*, Springer, Los Angeles, California, USA, **2004**.

[8] C. Brodman, Untersuchungen ueber Reibungkoeffizienten zu Fluessigkeiten. Dissertation, Goettingen, **1891.**

[9] C.L.M.H. Navier, Bull.Soc. Philomath., **1823**.

[10] J. Traube and S. H. Whang, Z.Physikal. Chem. A, **1928**, *138*, 102-122

[11] E. Schnell, J. Appl. Phys., **1956**, *27(1),* 1149-1152.

[12] P. Debye and R. L. Cleland, J. Appl. Phys., **1959**, *30*, 843-849.

[13] C. Chen, *J. Micromech. Microeng.* **2004**,*14*, 1091-1100.

[14] D. C. Tretheway and and C. D. Meinhart, *Phys. Fluids*, **2002**. *14(3)*, L9-L12.

[15] C. –H. Choi, J. Westin, K. Breuer. *Phys. Fluids,* **2003;** *15 (10)*, 2897-2902.

[16] T. D. Blake, *colloids Surf.,* **1990**, *47*, 135-145.

[17] E. Ruckenstein and P. Rajora, *Colloid Interface Sci.,* **1983**, *96*, 488-491.

[18] O. I. Vinogradova, *Int. J. Miner. Process*., **1999**, *56*, 31-60.

[19] J. R. Phillip, *J. Appl. Math. Phys*., **1972**, *23*, 353-372.

[20] P. deGennes, *Langmuir*, **2002**, *18*, 3413-3414.

[21] J. Tyrrell and P. Attard, *Langmuir*, **2002**, *18*, 160-167.

[22] G. Batchelor, An *introduction to fluid dynamics,* England, Cambridge University Press, **1967**.

[23] P. Tabeling, *Proc. 14th Australian Fluid Mechanics Conference*, **2001**, Adelaide, Australia.

[24] C. Choi, K. Johan, A. Westin, and K. S. Breuer, *Proc. IMECE200,* **2002**, New Orleans, Louisiana, USA.

[25] W. F. Ames, *Non-linear partial differential equations in engineering*, *vol 1* New York: Academic Press, **1967**.

[26] M. P. Arnal, D. J. Georing, and J. A. C. Humphrey, *J. Fluids Eng.,* **1991**, *113*, 384-398.

[27] C. A. J. Fletcher, Springer *Series in Computational Physics, vol 1* **2000**; pp. 362-368.

[28] S. Thakur, and W. Shy, *Numer. Heat Transf. Part B*. **1993,** *24*, 31-55.

[29] A. Mukhopadhyay, G. Biswas, and T. Sundarajan, *Int. J. Numer. Methods in Fluids* **1992**, *14*, 1473-1484.

[30] R. R. Hwang, and C. Yao, *J. Fluid Eng.* **1997**, **119**, 512-518.

Figure Caption:

1. Slip length for slip flow of liquid on solid surface
2. Microchannel for one-dimensional flow
3. Schematic of (a) p-control volume and (b) u-control volume
4. The arrangement of the computational grid in the computational domain, near the entrance of channel.
5. Comparison among Strouhal number (St) for the case of confined flow behind a square cylinder in a channel for blockage ratio $\frac{B}{H} = 0.25$.
6. The radial velocity (v) profile along radial direction through the channel.
7. Axial velocity (u) (a) at different values of x for $\mathrm{Re} = 10$, (b) along the centerline of the channel for different $\mathrm{Re} = 1, 10 \,\&\, 15$ and grid sensitivity shown at $\mathrm{Re} = 10$.
8. Axial velocity (u) along the centerline of micro, mini and macro channel.

.

9. The slip velocity (U_w) along the microchannel length.
10. The longitudinal pressure distribution at the channel centerline for different $\mathrm{Re} = (1, 10, 15)$.
11. The effect of slip on the value of *f. Re*

Table 1

Comparison of Strouhal number (St) and time-average drag coefficient ($\overline{C_D}$) at $\mathrm{Re} = 1000$ and for boundary layer thickness $\frac{\delta}{A} = 0.8, 0.5$ at various gap heights L.

Configuration		Strouhal number (St)			Drag coefficient ($\overline{C_D}$)		
$\frac{\delta}{A}$	L	Present	Hwang et al.[97]	% Error	Present	Hwang et al.[97]	% Error
0.8	5.5	0.121	0.122	1.64	1.99	1.98	0.50
	3.5	0.121	0.124	2.41	1.97	1.97	0.00
	1.5	0.132	0.135	2.22	2.13	2.14	0.46
	1.0	0.144	0.140	2.86	2.10	2.15	2.36
5.0	5.5	0.122	0.121	0.82	1.97	1.94	1.54
	3.5	0.106	0.111	4.50	1.64	1.66	1.21
	1.5	0.086	0.088	2.27	0.80	0.79	1.26
	1.0	0.083	0.080	3.75	0.52	0.50	4.00

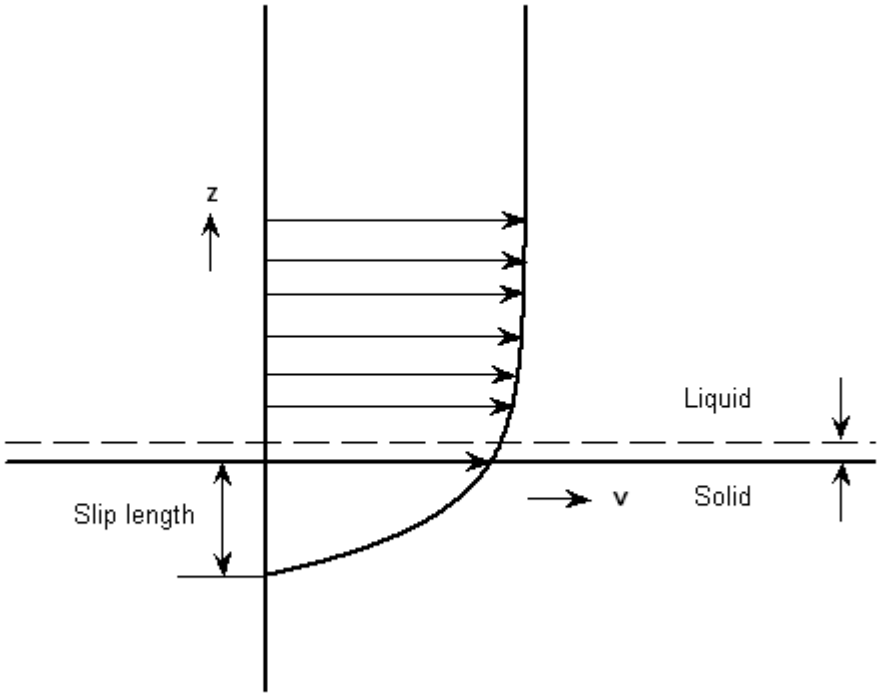

Fig. 1 Slip length for slip flow of liquid on solid surface

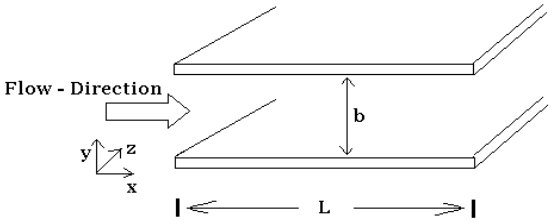

Fig. 2 Microchannel for one-dimensional flow

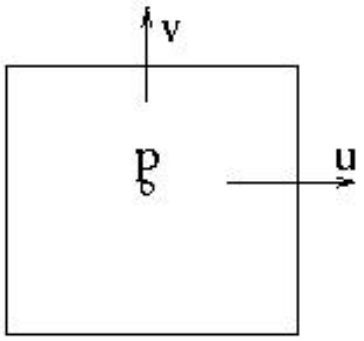

(a)

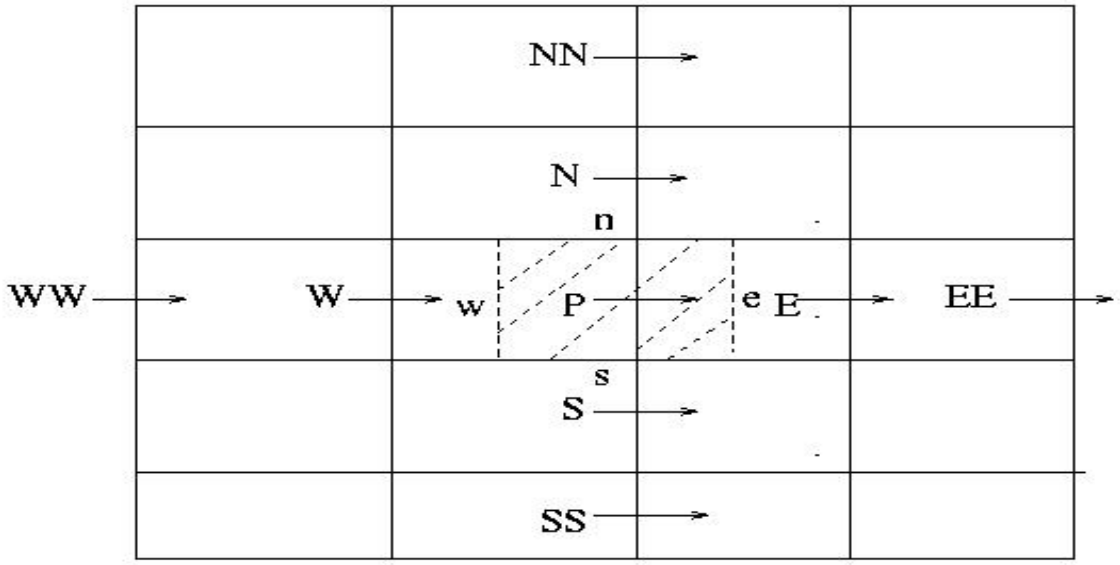

(b)

Fig. 3 Schematic of (a) p-control volume and (b) u-control volume.

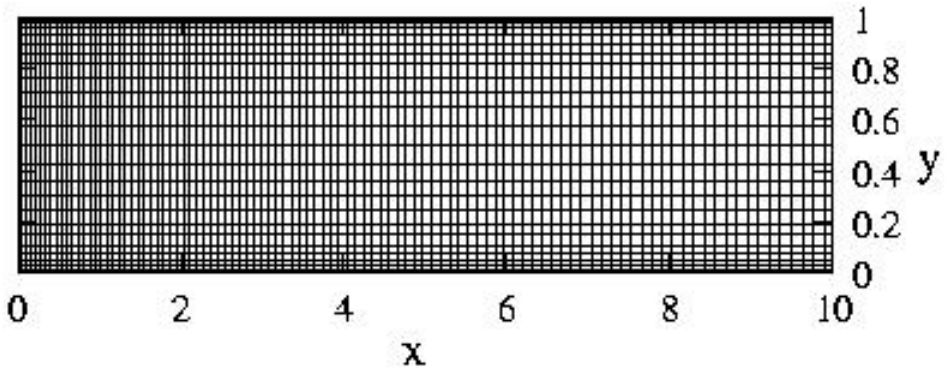

Fig. 4 **The arrangement of the computational grid in the computational domain, near the entrance of channel.**

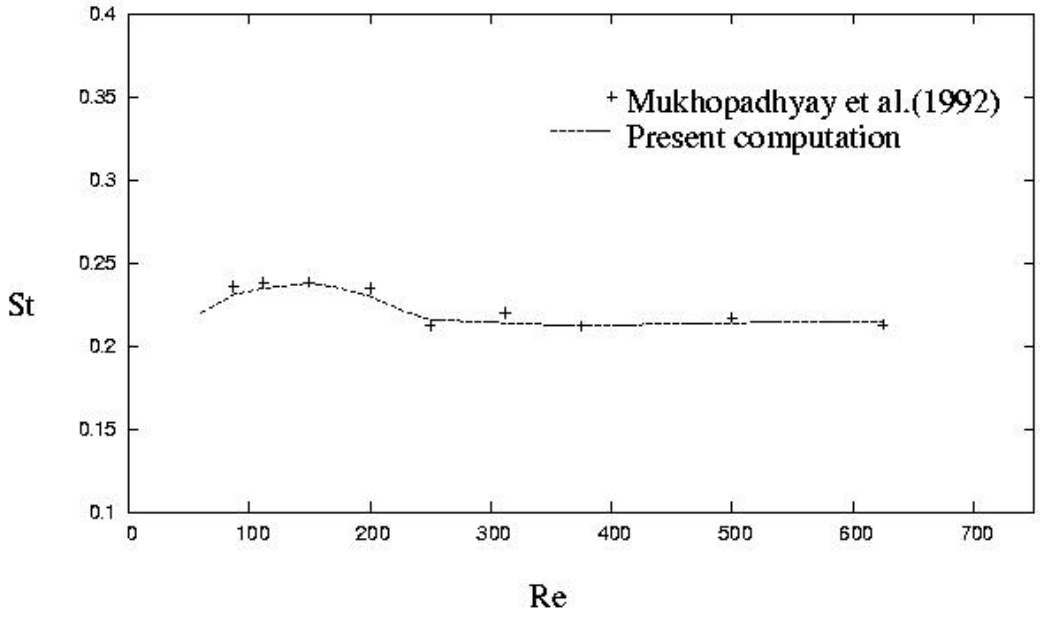

Fig. 5 **Comparison among Strouhal number (St) for the case of confined flow behind a square cylinder in a channel for blockage ratio $\frac{B}{H} = 0.25$.**

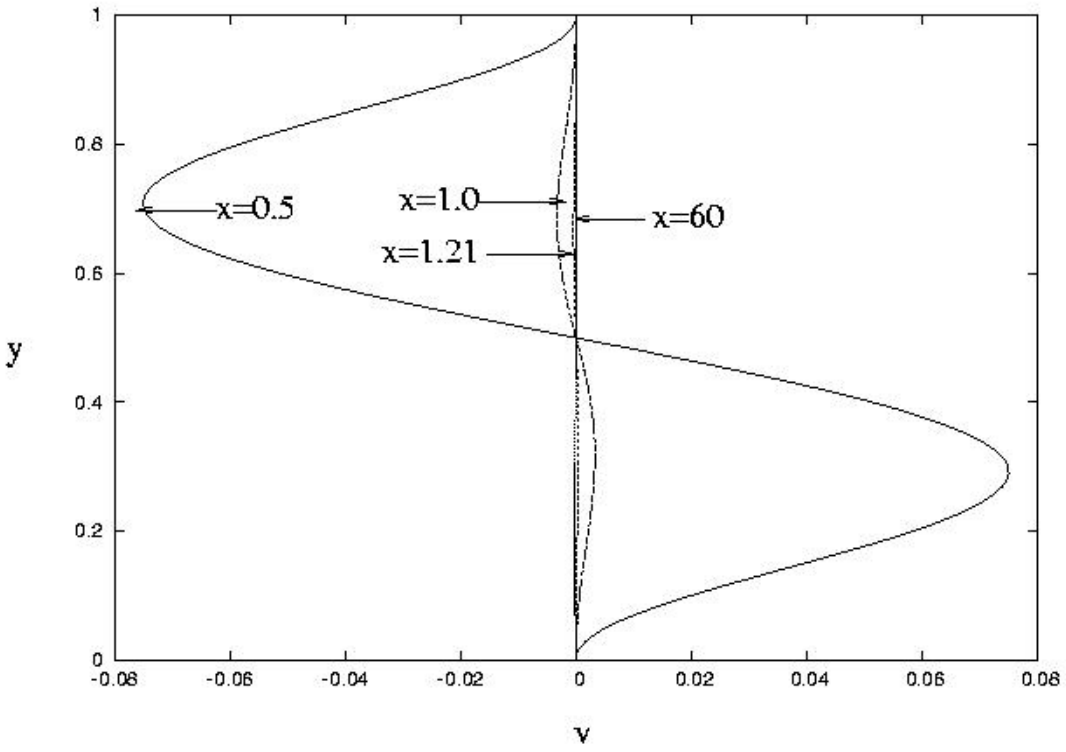

Fig. 6 **The radial velocity (v) profile along radial direction through the channel.**

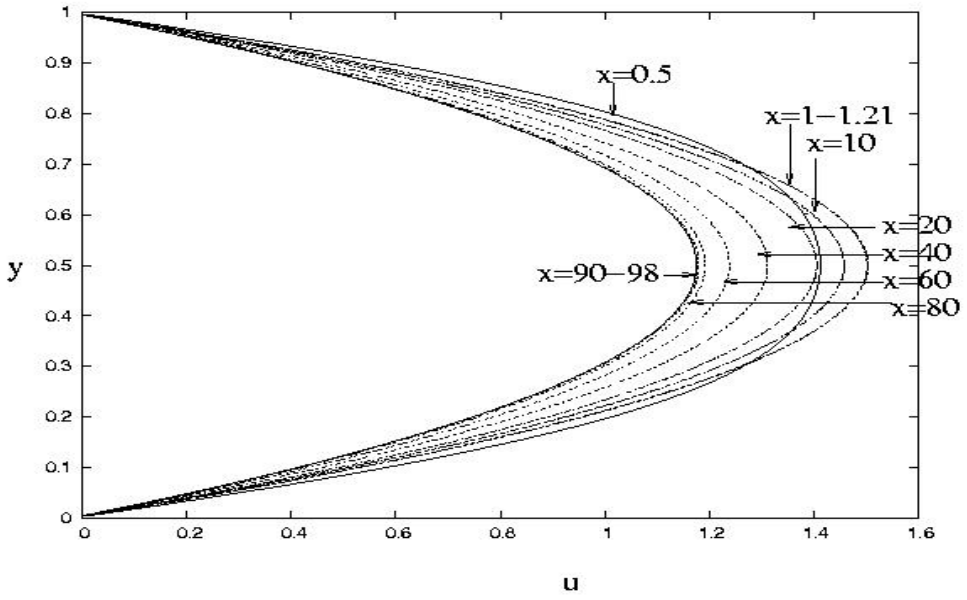

(a)

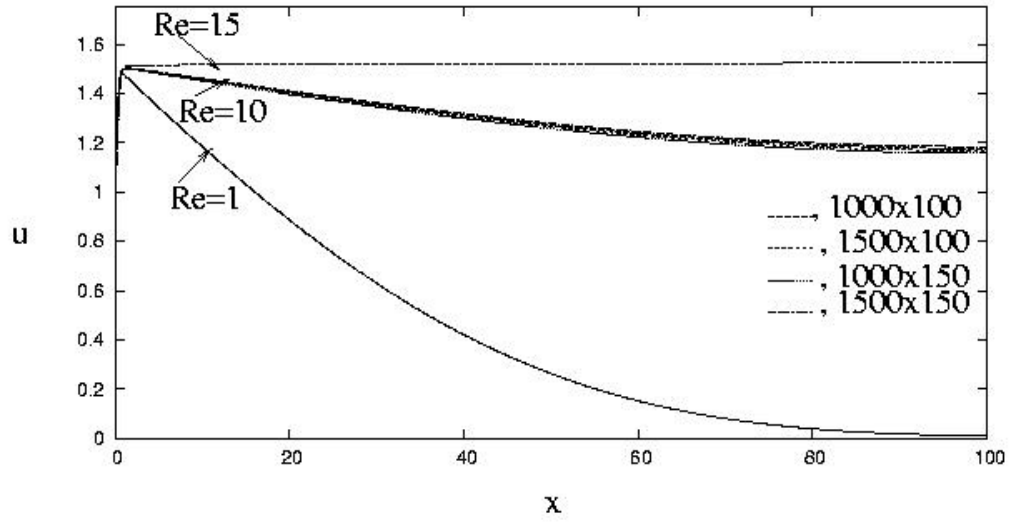

(b)

Fig. 7 **Axial velocity (u) (a) at different values of x for $\mathrm{Re} = 10$, (b) along the centerline of the channel for different $\mathrm{Re} = 1, 10 \,\&\, 15$ and grid sensitivity shown at $\mathrm{Re} = 10$.**

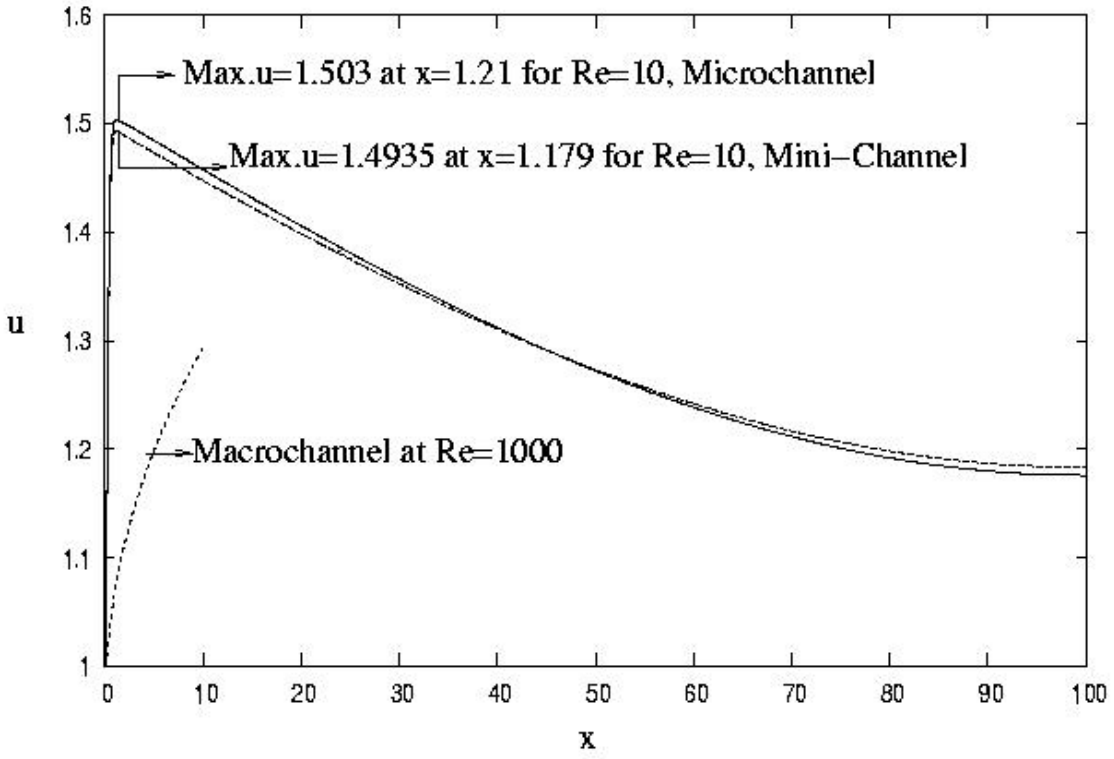

Fig. 8 **Axial velocity (u) along the centerline of micro, mini and macro channel.**

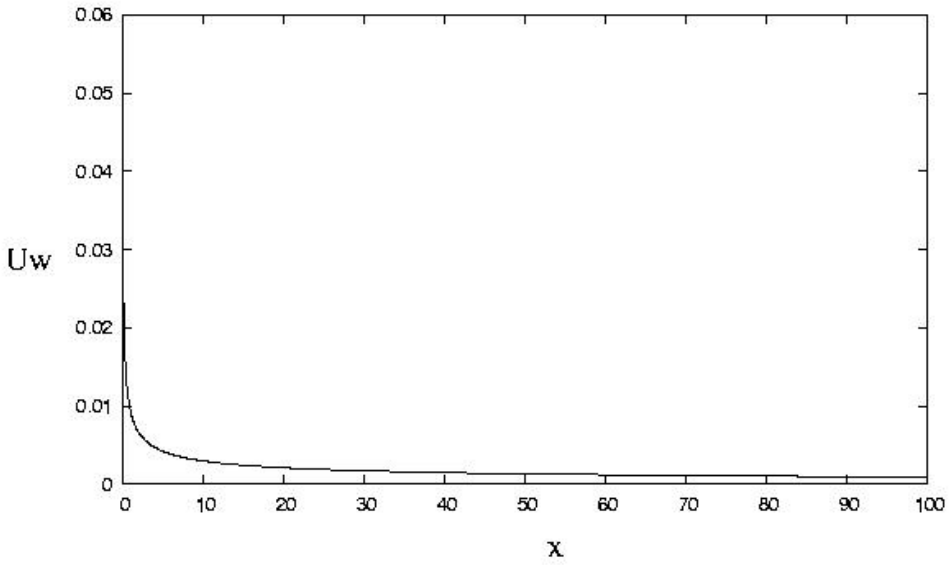

Fig. 9 The slip velocity (U_w) along the microchannel length.

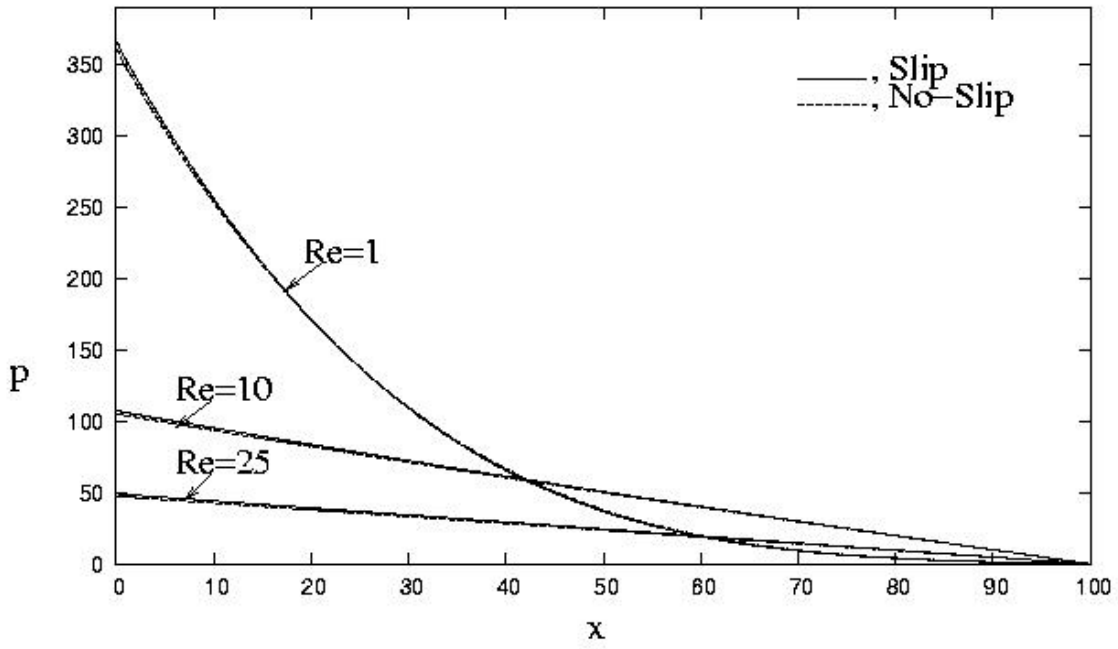

Fig. 10 **The longitudinal pressure distribution at the channel centerline for different Re = (1,10, 25) .**

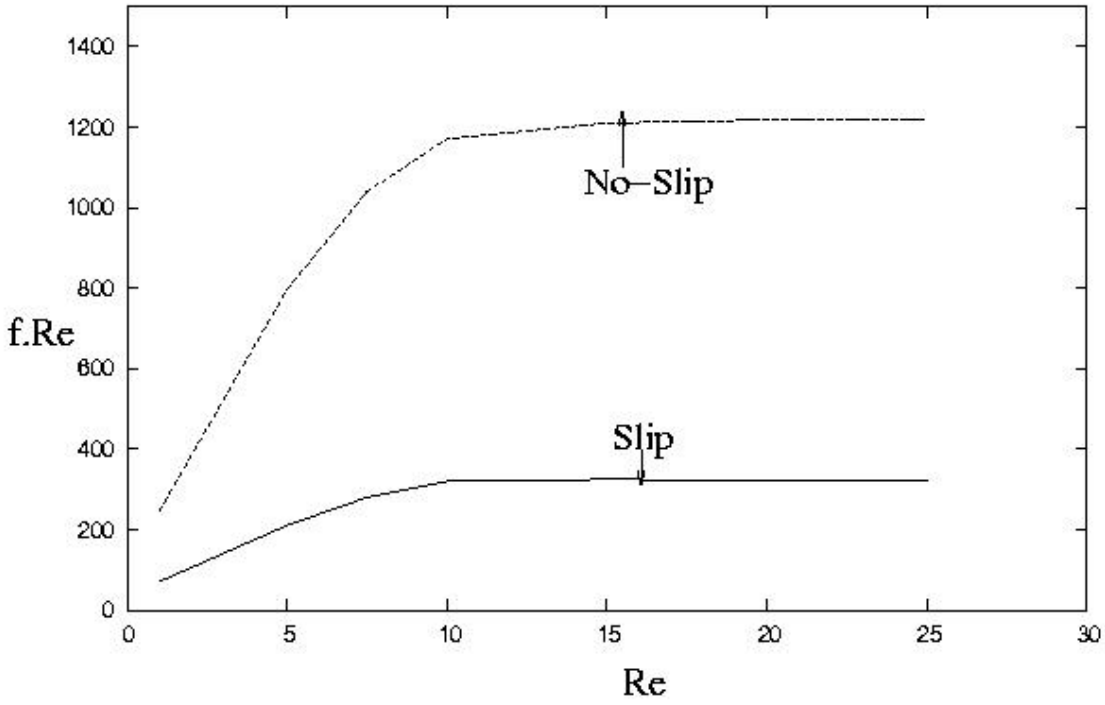

Fig. 11 The effect of slip on the value of *f. Re*